JOURNAL OF SPACECRAFT AND ROCKETS
Vol. 38, No. 1, January–February 2001

Computational Investigation of a Method to Compress Air Fluidically in Supersonic Inlets

Richard G. Haws,* Jeff S. Noall,† and Russell L. Daines‡
Brigham Young University, Provo, Utah 84602

The inlet is an important component in high-speed airbreathing engines. Whereas a variable-geometry inlet maximizes performance, it adds weight and complexity to the engine. Fixed-geometry inlets are limited to low contraction ratios to allow the initial normal shock to be swallowed and the engine to start. A novel fixed-geometry inlet configuration that uses a high-speed jet to act as the contact surface and compress the air is computationally investigated. Adjusting the jet pressure alters the contact surface and allows shock-on-lip conditions to be maintained over a range of flight Mach numbers without a movable flowpath. This configuration allows a low-blockage flowpath for low flight speeds, resulting in low spillage, while maintaining high compression in scramjet mode. Flow solutions are obtained using a Navier–Stokes solver. Flowfield details are presented and discussed, including the shock patterns and mixing between the jet and air. Shock-on-lip is demonstrated at varying flight Mach numbers, and associated effects on the flowfield are presented. Global analysis indicates that minimizing jet mass flow is a key to applying this concept to practical engines.

Nomenclature

a = speed of sound, m/s
b = shear-layer thickness, m
C_μ = turbulence constant, 0.09
C_{11} = turbulence constant, 1.0
C_{21} = turbulence model function, $0.5f + 0.055$
C_{22} = turbulence constant, 0.833
$\mathcal{D}$ = divergence of velocity
E = streamwise flux variables
e = total energy, J/kg
F = cross-stream flux variables
f = low-Reynolds-number damping function, $1 - \exp\{-0.022\rho q y/\mu\}$
k = turbulence kinetic energy, m^2/s^2
M = Mach number
M_t = turbulence Mach number, $\sqrt{2q/a}$
P = pressure, kPa
Q = vector of dependent variables
Q_v = viscous dependent variables
q = $\sqrt{k}$, m/s
r = freestream velocity ratio, U_2/U_1
S = strain-rate invariant
s = freestream density ratio, ρ_2/ρ_1
T = temperature, K
U = freestream velocity, m/s
u = streamwise velocity, m/s
v = cross-stream velocity, m/s
Y = mass fraction
y^+ = normal distance from surface in boundary-layer coordinates
ϵ = turbulence energy dissipation rate, J/s
μ = viscosity, kg/m-s
ρ = density, kg/m^3
ω = ϵ/k, specific rate of kinetic energy dissipation, s^{-1}

Subscripts

c = convective
i = incompressible
T = turbulence
1 = high-speed stream
2 = low-speed stream
∞ = freestream

Introduction

THERE is a growing demand for low-cost Earth-to-orbit and near-orbital flight vehicles. Some uses for Earth-to-orbit vehicles include satellite deployment and recovery, space-station maintenance, military applications, and eventually space tourism. Near-orbital flight offers fast long-distance travel for civilians, as well as advanced reconnaissance and long-range payload delivery for the military.

Scramjet engines have the potential to play a significant role in acceleration and cruise missions at these high speeds. The scramjet, or supersonic-combustion ramjet, engine is an experimental airbreathing engine proposed for use on hypersonic vehicles. The engine's distinguishing feature is supersonic combustion, which becomes necessary at hypersonic speeds to avoid extreme temperatures in which exothermic reactions are impossible were the flow subsonic.[1] In theory this engine is capable of delivering specific impulses two to four times greater than a rocket.

The inlet for a scramjet must achieve efficient compression and air capture over a wide Mach-number range. Although a large compression ratio is necessary at high Mach numbers for efficiency, less compression is needed at lower flight Mach numbers. Low compression is also necessary for starting the engine. If the engine is to operate in a low-speed mode, a large opening is needed with blockage minimized in order to maximize air capture. An example of an engine with these requirements is a turbine-based or rocket-based combined-cycle engine.[2] One fixed-geometry inlet design that has been proposed is the dual-mode combustion ramjet.[3] However, the dual-mode inlet does not meet the requirements for a low-speed mode because of the large associated blockage.

The low-compression requirements could be met in several ways. One way is with a variable-geometry inlet. Although this type of inlet can be controlled to yield the proper compression over a wide range of Mach numbers, variable geometry has the disadvantage of increased vehicle weight because of the machinery necessary for

Presented as Paper 99-0084 at the AIAA 37th Aerospace Sciences Meeting, Reno, NV, 11–14 January 1999; received 28 October 1999; revision received 15 May 2000; accepted for publication 17 May 2000. Copyright © 2000 by the authors. Published by the American Institute of Aeronautics and Astronautics, Inc., with permission.

*Graduate Student, Mechanical Engineering Department; currently Mechanical Engineer, Aeromechanics and Thermal Analysis Branch, U.S. Naval Air Warfare Center, Weapons Division, China Lake, CA 93555. Member AIAA.

†Graduate Student, Mechanical Engineering Department. Student Member AIAA.

‡Assistant Professor, Mechanical Engineering Department; daines@byu.edu. Member AIAA.

operation and increased complexity necessary to cool and seal the moving parts at high speed. An inlet with fixed geometry would be lighter and less complex than one with the variable geometry. This feature is especially important for Earth-to-orbit vehicles in which the entire dry weight of the vehicle must be carried to orbit. However, a low compression design would have poor high-speed performance. A typical fixed-geometry inlet is designed to achieve shock-on-lip at a single Mach number. Operating the inlet below this design Mach number results in spillage, resulting in increased drag and decreased air capture by the inlet. Operation above the design Mach number causes "overspeeding" the inlet, which results in a loss of potential compression and performance in the engine. The present research is motivated by the desire to achieve low spillage at low Mach numbers and high compression at high Mach numbers without the incorporation of variable geometry.

Overview of Fluidic Compression

A fixed-geometry inlet concept that uses a high-speed jet acting as the compression surface to compress the inlet air is referred to as a fluidic compression inlet in the present work. This inlet shares similarities with a traditional fixed-geometry scramjet inlet, but there are also significant differences.

A diagram of a fixed-geometry scramjet engine with a two-shock, mixed compression inlet is shown in Fig. 1. Incoming air is compressed in the inlet and isolator. The supersonic air then enters the combustor, where fuel is added and burned. The gases are then expanded and accelerated in a nozzle.

In the fluidic compression inlet (Fig. 2) the compression ramp of the traditional inlet has been replaced by a gas stream, angled relative to the incoming flow and at a higher pressure than the inlet air. This gas stream, referred to as the compression jet, could be produced by a gas generator, rocket exhaust, or other onboard sources such as fuel or oxidizer. The virtual compression surface created by the compression jet ends at a splitter plate, which separates the air from the jet flow. At design conditions both the shear layer between the jet and air and the shock from the cowl lip impinge on the leading edge of the splitter plate. The air enters an isolator and then a combustor region. Below the splitter plate the lower jet wall is turned horizontal at a point where the expansion fan will land at or downstream from the leading edge of the splitter plate. Downstream from the splitter plate both the airstream and the jet are expanded in a nozzle, producing thrust.

The fluidic compression process can be understood using standard compressible flow theory. When the airflow and the jet flow meet, an oblique shock forms to turn the airstream, resulting in a pressure increase in the air. The same external shock angle is desirable for all flight conditions so that the shock extends to the lip of the engine cowl for full air capture. Behind this shock the two streams must satisfy the conditions of equal pressure and common flow direction, which will result in compression or expansion waves if the streams are at different pressures or flow angles. There is a unique combination of waves that will satisfy the conditions of matched pressure and flow direction, as explained next. The adjustment process effectively provides a dynamically adjustable contact surface and is a key difference between fluidic and traditional inlets.

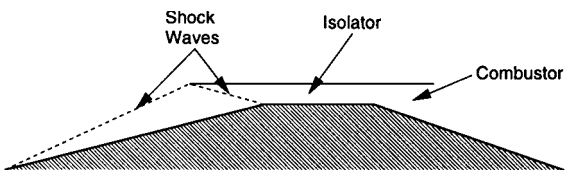

Fig. 1 Schematic diagram of scramjet engine with fixed-geometry two-shock mixed compression inlet.

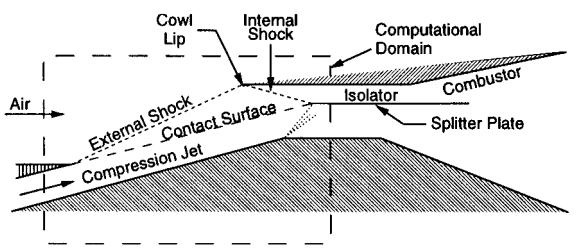

Fig. 2 Schematic diagram of fluidic compression inlet and computational domain for present work.

Three cases are used to illustrate the processes involved. At on-design conditions turning the airflow by an angle equal to the angle of the jet flow results in an oblique shock that will land on the cowl lip. The jet pressure is chosen to be equal to the pressure of the inlet air after going through the oblique external shock. Because both the pressure and flow angle of the two flows are matched, no further adjustment of the flows occurs after the shock. The jet will remain at constant pressure as a result of the constant-area flowpath.

When a traditional inlet is operating below the design flight Mach number, the external shock will land upstream of the cowl lip, resulting in spillage and lower mass capture. In a fluidic compression inlet the jet pressure can be reduced to decrease the angle of the external shock such that it lands on the cowl lip. Maintaining shock-on-lip under these conditions results in a turning angle of the air that is less than the jet angle, causing a shock to form that turns and compresses the jet. A reflected shock off the lower wall will further compress and turn both the jet and the air downstream from the external shock.

At flight Mach numbers above design conditions, the external shock will land downstream of the cowl lip in a traditional inlet, which could result in flow separation and possibly engine unstart. In the fluidic compression inlet the jet will then be operated at elevated pressures to increase the angle of the external shock and maintain shock-on-lip. The air is then turned at an angle greater than the jet inlet angle, and an expansion fan will form in the jet to cause it to match the airflow angle. This expansion fan will reflect off the lower wall and expand and turn both the jet and the air downstream from the external shock. By operating with varying pressures over a range of Mach numbers, the compression jet will allow the inlet to behave as a variable geometry inlet by keeping the shock placed on the cowl lip.

Potential Benefits of Fluidic Compression

Fluidic compression results in several potential benefits. One of the important benefits is the small associated physical area contraction with a large effective contraction for high internal compression at high flight Mach numbers. The contraction ratio is defined as the ratio of the capture area of the inlet to the flow area in the isolator. The calculation of the inlet area assumes full mass capture, that is, a streamline extends horizontally to the cowl. For a fluidic compression inlet with the jet off, the areas both above and below the splitter plate would act as the isolator, resulting in a low physical contraction ratio. This low contraction ratio would allow for greater mass capture at low Mach numbers. This greater mass capture would improve the performance of combined-cycle engines during ejector and ramjet modes. The low physical contraction ratio also makes it possible to start the inlet for higher-Mach-number flight. Conventional fixed-geometry inlets are limited to low contraction ratios to enable engine starting. With the jet on, the jet fills the flow area below the splitter plate, reducing the airflow area to the region above the splitter plate and resulting in a significantly higher effective contraction ratio. Larger contraction ratios improve engine specific impulse at high flight Mach numbers.

Other benefits include an improvement of off-design mass capture through the ability to control the position of the external shock and maintain the shock-on-lip condition over a range of Mach numbers. The compression jet also augments the thrust of the engine.

By using fluidic compression the problem of engine unstart resulting from the internal shock wave causing boundary-layer separation could be reduced. Boundary layers exist immediately upstream of the point where the jet and the inlet airstream meet. As the shear layer develops between the airstream and the compression jet, the low-momentum fluid from the boundary layers is accelerated. When this flow encounters the splitter plate, the velocity is supersonic with a smooth transition across the contact surface. The flow at the leading edge of the splitter plate is less likely to separate where the shock from the cowl lip impinges, and any boundary-layer

separation caused by the internal shock wave cannot propagate upstream of the splitter plate to cause unstart.

Potential Drawbacks of Fluidic Compression

There are drawbacks associated with fluidic compression caused by the presence of a splitter plate and the increased propellant used to produce the jet flow. One of the difficulties associated with the splitter plate is that the optimum location of the splitter plate changes with varying Mach numbers. At the optimum location the splitter plate performs three functions: separation of the compressed air from the compression jet, prevention of the expansion fan from the lower jet wall from expanding the compressed air, and interception of the internal shock wave, which emanates from the cowl lip, preventing shock losses in the jet flow.

The simultaneous realization of these three functions can only occur at a single flight Mach number when the shear layer, the internal shock, and the expansion from the lower wall all intersect at a single point; at all other flight conditions multiple intersection points will exist. Two options in designing the splitter plate location are explored here: a translating splitter plate to somewhat optimize performance, or a stationary splitter plate. The motion of a translating splitter plate can be limited to sliding along a predetermined path. Even this simple motion, however, would require moving parts and increase the vehicle weight and complexity. Furthermore, translating the splitter plate can, in general, only optimize two of the three functions it performs because the shock, shear layer, and expansion will not intersect at a single point for off-design conditions.

The location of a fixed splitter plate depends on the relative importance of several off-design loss mechanisms. If the splitter plate were too far downstream, the shock from the inlet cowl could enter the jet flow at low flight Mach number conditions, causing shock losses, whereas at other conditions the expansion fan from the lower corner could enter the airflow, decreasing air compression. Below the design Mach number the jet will be compressed by the inlet air behind the external shock, as just discussed, and will decrease the cross-sectional area of the jet stream tube and cause some of the inlet air to flow under the splitter plate and not enter the combustor. Above the design Mach number the jet will expand behind the external shock, allowing some of the jet gases to flow above the splitter plate and mix with the airflow. This effect could provide some benefits. The additional gas effectively increases the compression. It may be possible to introduce free radicals in the combustor, helping to initiate combustion, if a combustion process is used to produce the compression jet. If the jet contained fuel, some of the fuel for the airstream could be injected in this way. However, if this fuel reacts before reaching the isolator, the resulting flow and pressure fields would be altered with undesirable effects possible, such as increased flow blockage.

There are other drawbacks associated with the presence of a splitter plate. The plate increases the wetted area, causing increased viscous losses. Furthermore, a physical splitter plate will have a finite thickness, which will cause shocks to form and therefore increase shock losses. The leading edge of the splitter plate also presents significant cooling challenges. Further research is required in each of these areas.

Although providing significant benefits, the jet flow itself has penalties associated with it. If all of the jet flow comes from onboard fuel, oxidizer, or both, the specific impulse of the jet flow will be lower than that of the main scramjet flow, reducing the overall engine specific impulse. The jet flow can also experience shock losses when the splitter plate ends and the flows again join. For fluidic compression to be feasible for a scramjet inlet, the improved performance of the main flow and the weight reduction from the use of a fixed-geometry inlet must offset the penalties of the splitter plate and jet flow.

Solution Technique and Problem Description

Modeling of fluidic compression is accomplished by iteratively solving the Navier–Stokes equations in a coupled manner using a diagonalized alternating-direction implicit (ADI) algorithm based on a scheme introduced by Pulliam and Chaussee.[4] In the diagonalized ADI algorithm the left-hand-side inversion is simplified to a series of scalar inversions and matrix multiplication by diagonalizing the Jacobians of the flux vectors, compared to the block inversions necessary in full ADI schemes. This simplification significantly reduces the number of operations and CPU time required. The diagonalized ADI algorithm has been implemented in a number of codes, including ARC2D and ARC3D,[5] NPARC,[6] WIND,[7] and UTNS,[8] as well as the code used in the present work.[9]

The Navier–Stokes equations are written in vector form in two dimensions as

$$\frac{\partial Q}{\partial t} + \frac{\partial E}{\partial x} + \frac{\partial F}{\partial y} = L(Q_v) + H \tag{1}$$

where the vectors Q, E, and F are comprised of the terms for the continuity, momentum, energy, species, and turbulence equations in conservative form. These vectors are given in Eq. (2):

$$Q = \begin{pmatrix} \rho \\ \rho u \\ \rho v \\ e \\ \rho Y_i \\ \rho q \\ \rho \omega \end{pmatrix}, \qquad E = \begin{pmatrix} \rho u \\ \rho u^2 + p \\ \rho u v \\ u(e+p) \\ \rho u Y_i \\ \rho u q \\ \rho u \omega \end{pmatrix}$$

$$F = \begin{pmatrix} \rho v \\ \rho u v \\ \rho v^2 + p \\ v(e+p) \\ \rho v Y_i \\ \rho v q \\ \rho v \omega \end{pmatrix}, \qquad Q_v = \begin{pmatrix} p \\ u \\ v \\ T \\ Y_i \\ q \\ \omega \end{pmatrix} \tag{2}$$

$L(Q_v)$ in Eq. (1) represents the viscous terms written in terms of Q_v, which simplifies the form of the viscous coefficient matrix. A two-equation $q-\omega$ turbulence model is included.[10] The source vector H contains the turbulence source terms and species and energy source terms for reacting flows. The turbulence source terms are given by

$$H_q = \tfrac{1}{2}\left[C_\mu f(S/\omega^2) - \tfrac{2}{3}(\mathcal{D}/\omega) - C_{11}\right]\rho\omega q \tag{3}$$

$$H_\omega = \left\{C_{21}\left[C_\mu(S/\omega^2) - \tfrac{2}{3}(\mathcal{D}/\omega)\right] - C_{22}\right\}\rho\omega^2 \tag{4}$$

A turbulence viscosity

$$\mu_T = C_\mu f(\rho q^2/\omega) \tag{5}$$

is computed from the turbulence variables. The inclusion of this turbulence viscosity in the viscous dissipations terms of the momentum, energy, and species equations couples these equations with the turbulence model. In the thermal and species diffusion terms the turbulence viscosity is divided by a turbulence Prandtl and Schmidt number with values of 0.9 and 1.0, respectively.

For the fluidic compression inlet a key physical feature is the high-speed shear layer between the air and compression jet. High-speed compressible shear layers tend to grow more slowly than their incompressible counterparts. The growth rate of an incompressible shear layer is given by[11]

$$\left(\frac{\mathrm{d}b}{\mathrm{d}x}\right)_i = 0.165\frac{(1-r)\left(1+\sqrt{s}\right)}{2\left(1+r\sqrt{s}\right)} \tag{6}$$

The growth rate of a compressible shear layer is also a function of the convective Mach number

$$M_c = (U_1 - U_2)/(a_1 + a_2) \tag{7}$$

with the growth rates decreasing as the convective Mach number increases. To account for the decrease in growth rates, the turbulence source terms are modified by subtracting a correction factor $1.5M_t^2 - 0.09375$ from both C_{11} and C_{22} (Ref. 12).

A number of features of the code are important in the present work. Inviscid and viscous time-step preconditioning are included, as well as a total-variation-diminishing scheme to resolve shocks. Because of the importance of boundary layers in this application, viscous wall boundary conditions are used. The turbulence model is integrated to the wall, with the first grid point away from the wall placed within $y^+ = 3$. Third-order upwind-biased spatial discretization is used for all results presented. Supersonic inlet boundary conditions are specified at the air and jet flow inlets, with the Mach number, flow angle, species concentrations, and stagnation temperature and pressure specified. Exits are supersonic, with flowfield properties extrapolated from inside the computational domain.

Predictions generated using this code have been compared to wall-pressure profiles in a high-speed ejector where the two streams were supersonic and high-subsonic, respectively. The rate of mixing of the streams plays an important role in the resulting wall-pressure profiles. Close agreement between predicted and measured wall pressures implies that the mixing is being modeled adequately. Predicted wall pressures matched experimentally measured pressures to within 6.4% on average.[13] This level of agreement gives confidence in the predicted mixing rates in the present work.

All domains in the present work are two-dimensional. As seen in Fig. 2, the computational domain begins slightly upstream of where the jet is introduced and extends downstream of the leading edge of the splitter plate. The air inlet conditions are derived from the freestream conditions of a trajectory analysis for a representative vehicle. The inlet flow properties are calculated using shock theory across a forebody shock produced by a forebody half-angle of 7.5 deg, assuming a calorically perfect gas with a specific heat ratio of 1.4. These properties are applied at the model inlet. Three flight Mach numbers were studied: 4.7, 6.0, and 9.2, which correspond to Mach numbers at the beginning of the inlet of 4.0, 5.0, and 7.0, respectively. The 4.7 value chosen here is close to the minimum flight Mach number at which a scramjet can operate on a 2000-psf trajectory. The jet pressure in each case is adjusted to locate the external shock on the cowl lip. A typical rocket combustion chamber stagnation temperature 3200 K is used for the gaseous H_2O jet. The jet enters at an inclination of 14 deg to the airflow.

The grid used has 450 points in the cross-stream direction and 606 points in the streamwise direction and is shown in Fig. 3. Grid points are clustered near solid-wall boundaries, and for many of the cases the grid is adapted to cluster points near regions of high gradients in pressure and velocity. The upper surface of the model upstream of the engine cowl is extended vertically, and a solid wall boundary condition is applied. The model was set up this way and physical dimensions chosen in support of potential direct-connect (as opposed to freejet) experiments of this concept, which have not yet occurred. The extended region provides sufficient space for removal of the boundary layer to simulate freestream conditions at the cowl.

In the present work a two-shock, mixed-compression inlet with a 14 deg compression ramp, designed for operation at an inlet Mach number of 5, has an overall contraction ratio of 3.90. All cases shown are for a jet Mach number of 2.0 and a jet-to-capture-area-ratio of 0.271. The jet width studied could result in a physical (jet-off) contraction ratio as low as 1.59 assuming the expansion in the compression jet just touches the leading edge of the splitter plate as in Fig. 2. In this work, however, turning of the lower jet wall to horizontal is delayed until directly below the leading edge of the splitter plate, as seen in the grid in Fig. 3, in order to ensure that the expansion does not affect the airflow. This delay results in a higher physical contraction ratio of 1.87.

In the following section the on-design jet compression process will first be described. The effects of flight Mach number on the flow will then be discussed. The effects of compression jet width and Mach number will be discussed, as well as grid resolution. Finally, a global analysis of one potential application, a fixed geometry inlet for hypersonic acceleration or cruise, will be analyzed.

Results

The pressure contours for a flight Mach number of 6 (Fig. 4) clearly demonstrate the shock system that develops in this inlet. There are two main areas of interest: the region immediately following the initiation of the external shock where the contact surface begins to develop and the isolator section immediately following the internal shock. This figure clearly demonstrates the external shock formed as the two fluid streams meet. Behind the shock the jet and air pressure match. This shock intercepts the cowl lip, which is expected at on-design conditions. At that point the internal shock forms, which extends down to the splitter plate and redirects the airflow parallel to the isolator walls. The splitter plate was not perfectly positioned, as the shock intersects aft of the leading edge. Ideally the shock would fall on the leading edge of the splitter plate. In the lower jet a shock wave is seen to form at the leading edge of the splitter plate. This shock terminates at the point where it meets the expansion fan emanating from the lower corner point. The pressure in the jet below the splitter plate is significantly lower than the pressure in the isolator.

The contours of horizontal velocity for a flight Mach number of 6 are shown in Fig. 5. The contact surface can be seen by the contours beginning at the flow merge point and extending to the splitter plate. The jet flow remains at a fairly constant velocity. Because of the differences in temperature, velocity, and gas composition, there is also a Mach-number difference across the contact surface with an air Mach number of 3.5 and a jet Mach number of 2.0. For these conditions the velocity ratio r is 0.68, and the convective Mach number is 0.47. Although the air Mach number is higher, the air velocity is lower than that of the jet. The boundary layer on the upper surface is not affecting the flow into the inlet.

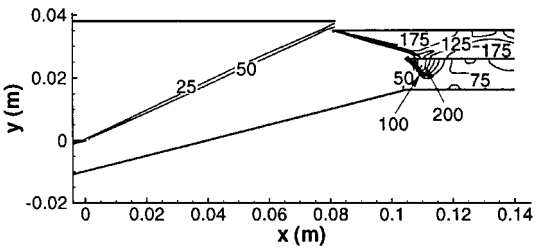

Fig. 4 Pressure contours in fluidic compression inlet; $M_\infty = 6.0$. (Contour interval is 25 kPa.)

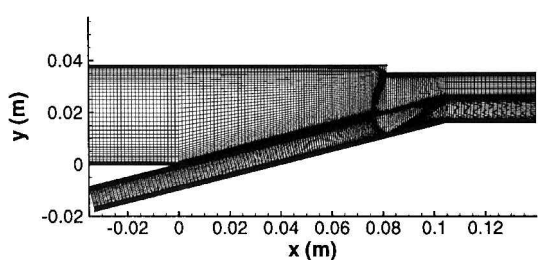

Fig. 3 Computational grid for fluidic compression model (jet to capture area ratio of 0.271).

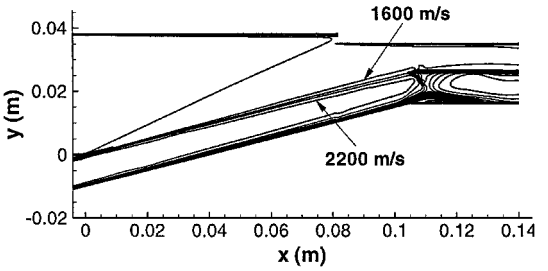

Fig. 5 Contours of horizontal velocity in fluidic compression inlet; $M_\infty = 6.0$. (Contour interval is 200 m/s.)

Mixing

Some turbulent mixing is expected to occur at the contact surface because of the velocity gradient that exists there. An examination of the flowfield provides an understanding of the degree to which the jet flow mixes with the airflow. This mixing can cause some of the unburned air from the inlet to flow below the splitter plate, degrading performance by reducing the amount of energy that can be added in the combustor and reducing the thrust that can be produced. A small amount of mixing does, however, have the beneficial effect of accelerating the low-speed flow from boundary layers in the air and jet flows. Three types of mixing in the shear layer will now be discussed: momentum exchange, thermal mixing, and diffusion of chemical species. For purposes of measuring mixing layer thicknesses, all mixing layers are assumed to begin where properties have changed by 10% of the difference between the bulk flow properties in the air and the jet flow.

From the velocity vectors at the merge point shown in Fig. 6, it is seen that the boundary layers in the air and the jet quickly reaccelerate and the shear layer velocity profile becomes smooth. The increased vector density in the shear region reflects the increased local grid density.

Figure 7 shows the velocity vectors in the shear layer just before the splitter plate. As the air enters the isolator, there is no boundary layer present as there would be if a solid wall replaced the contact surface. For this reason this inlet should be less likely to unstart than a traditional inlet. Momentum mixing is more pronounced than either thermal or species diffusion. In Fig. 5 the growth of the momentum

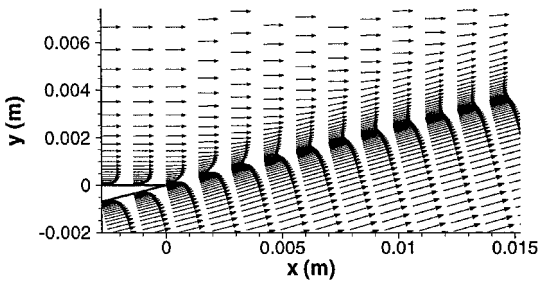

Fig. 6 Velocity vectors near jet-air merge point at beginning of contact surface; M_∞ = 6.0. (Vector density indicates grid spacing.)

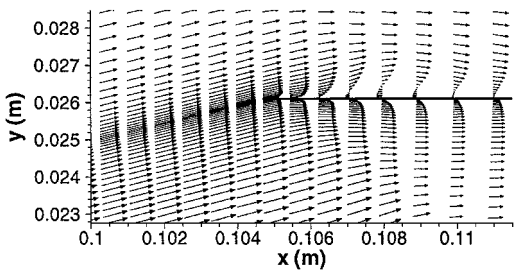

Fig. 7 Velocity vectors at end of contact surface and beginning of splitter plate; M_∞ = 6.0. (Vector density indicates grid spacing.)

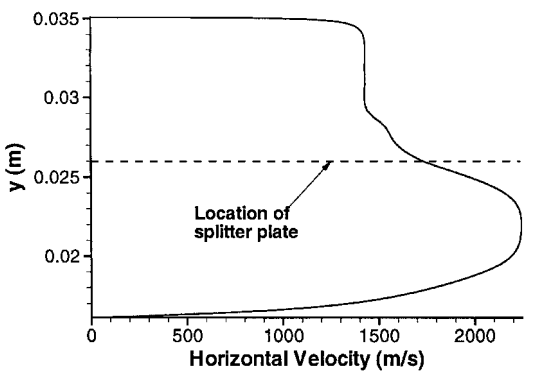

Fig. 8 Horizontal velocity profile immediately before splitter plate leading edge; M_∞ = 6.0.

Table 1 Variation of pressure and Mach number of airflow through the computational domain over a range of flight Mach numbers (Mach 2 compression jet)

Inlet parameter	$M_\infty = 4.7$	$M_\infty = 6.0$	$M_\infty = 9.2$
Mach number			
Freestream	4.7	6.0	9.2
Air inlet	4.0	5.0	7.0
After external shock	3.1	3.6	4.5
After internal shock	2.4	2.8	3.4
Pressure, kPa			
Freestream	6.55	4.46	2.08
Air inlet	14.8	12.3	8.9
After external shock	54	59	65
After internal shock	150	180	260
Jet pressure, kPa	34	60	86
Air compression ratio	23	40	125
Velocity ratio, r	0.59	0.68	1.0
Convective Mach number	0.53	0.47	0.0

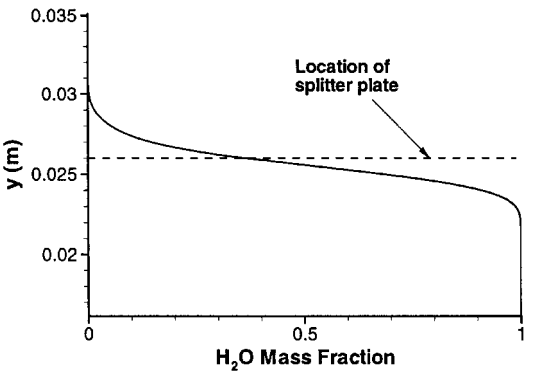

Fig. 9 Cross-stream profile of H_2O molar concentration near splitter plate leading edge; M_∞ = 6.0.

mixing layer can be seen from the spread of the velocity contours near the contact surface, whereas the velocity profile in Fig. 8 shows the extent of momentum mixing immediately upstream of the splitter plate. At this point the momentum mixing layer is approximately 4.5 mm wide or 18% of the total duct width. The shear-layer growth rate db/dx is 0.0269, which is 77% of the incompressible growth rate. This value agrees with experimentally measured growth rates, which range between about 60% to just under 100% for convective Mach numbers around 0.5 (Ref. 11).

The water mass fraction profile immediately before the splitter plate in Fig. 9 shows that the species diffusion layer has grown to about 3.4 mm or 14% of the total duct width. There is diffusion of air into the jet flow, and it can be seen that some air flows below the splitter plate. For these conditions just under 11% of the airflow goes under the splitter plate. A temperature profile is not shown; however, thermal diffusion was less pronounced than momentum or species mixing, with a mixing layer 3.1 mm wide or 13% of the duct width.

Effect of Flight Mach Number

Table 1 shows Mach number and pressures at different locations in the airflow over a range of flight Mach numbers for a Mach 2 compression jet. As the flight Mach number increases, the freestream pressure decreases (for the flight trajectory considered), as well as the pressure behind the assumed forebody shock. However, after the external shock pressures are higher for higher flight Mach numbers, indicating a strengthening shock as flight Mach number increases. The increase in pressure with flight Mach number is more pronounced after the internal shock; therefore, the net result of increasing the flight Mach number is an increase in the overall compression ratio. In the isolator Mach numbers range from 2.4 to 3.4 for these flight conditions. Jet pressures and air compression ratio for the varying Mach numbers are also shown, along with the flow velocity ratio between the jet and the air across the contact surface. The jet pressure and air compression ratios increase with increasing

flight Mach number, while the velocity ratio between the jet and air decreases.

Fluidic compression gives control over the location of the external compression shock wave to improve air mass capture at low Mach numbers and high-Mach-number inlet performance. Low-Mach-number mass capture is one of the most important parameters affecting mission-average specific impulse of scramjet engines. As the shock-on-lip condition is maintained at various flight Mach numbers, the angle of the internal shock will change; other flow characteristics are also expected to change. Figure 10 shows the pressure contours in the region of the cowl lip and splitter plate at flight Mach numbers of 4.7 and 9.2. Table 1 indicates the jet pressures required to achieve shock-on-lip conditions for these cases. Shock patterns are similar to those at the design condition. Most

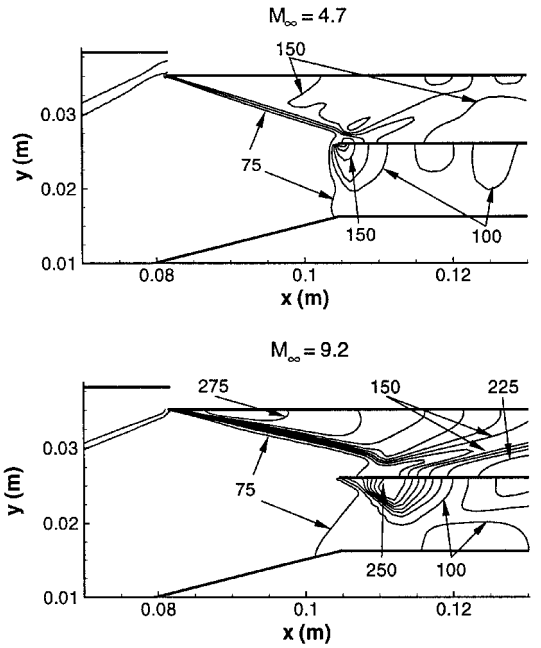

Fig. 10 Pressure contours near splitter plate in fluidic compression inlet; M_∞ = 4.7 and 9.2. (Contour interval is 25 kPa.)

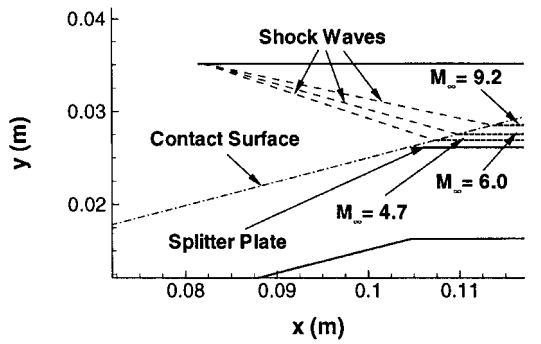

Fig. 11 Fixed splitter plate location in present work and optimum locations for a movable splitter plate; M_∞ = 4.7, 6.0, and 9.2.

importantly, shock-on-lip was achieved both below and above the inlet design Mach numbers by adjusting the jet pressure. Below the design Mach number this jet adjustment prevents spillage from occurring and increases the airflow through the engine. Above the design Mach number it prevents the losses associated with overspeeding. These numerical results demonstrate that fluidic control of this inlet without variable geometry can be attained—one of the benefits of this inlet scheme. Continuous control of the jet pressure is achievable, providing good control possibilities for this type of inlet.

Two phenomena will be discussed that result from maintaining shock-on-lip which affects the airflow entering the isolator. The first is a change in internal shock angle, and the second is a displacement of the contact surface. As the Mach number behind the first shock increases with increasing flight Mach number, the slope of the shock coming off the cowl lip decreases relative to the isolator wall; this shock lands farther downstream on the splitter plate. In the cases shown here, the shock always lands downstream of the leading edge, preventing it from entering the jet flow. The pressure contours in Fig. 10 show that at a flight Mach number of 4.7 the internal shock is near the edge of the splitter plate. The shock extends further into the isolator region at flight Mach numbers of 6.0 (Fig. 4) and 9.2. One way to maintain the shock on the leading edge of the splitter plate would be to introduce limited variable geometry into this inlet by allowing the splitter plate to translate. The optimum location for the leading edge of the splitter plate would be where the contact surface and internal shock intersect. This location is shown in Fig. 11 for the flight Mach numbers presented in this work. The splitter plate must move downstream and toward the cowl as the flight Mach number increases in order to achieve this condition. This movement represents an opportunity to improve performance by increasing the compression at high Mach numbers through the use of a translating splitter plate. Conversely, not having the splitter plate leading edge at the shock-contact surface intersection represents lost potential for compression in a fixed-geometry design.

When the internal shock wave lands behind the leading edge of the splitter plate, the shock causes a small separation region between itself and the plate leading edge (as shown in Fig. 7). However, the separation cannot propagate farther upstream, which reduces the risk of unstart from shock-induced boundary-layer separation at high contraction ratios.

Another result of operating at off-design Mach numbers is that the airflow has not been turned parallel to the jet when the two streams initially come into contact. This phenomenon was just discussed and results in a compression or expansion of the jet flow. The pressure contours for all three flight Mach numbers near the jet entrance region are shown in Fig. 12. At on-design conditions $M_\infty = 6.0$, the pressure of the jet is nearly matched to the pressure behind the shock (a slight expansion occurs in the jet). At Mach 4.7 conditions the turning angle of the flow through the shock is less than the jet flow angle; therefore, a shock forms in the jet and reflects off the lower wall. The first shock turns the jet flow downward, and the reflected shock turns both flows parallel to the lower wall. These shocks also compress the jet and air as can be seen by the pressure contours. Table 1 indicates that the jet pressure had to be set significantly lower than the air pressure behind the external shock so that the pressures would be properly matched after the jet shock. At Mach 9.2 conditions the external shock turns the airflow too much. An expansion fan is formed in the jet flow, turning it upward so that it

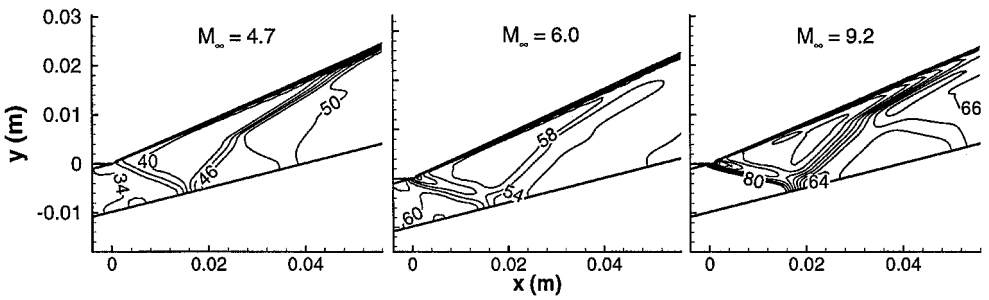

Fig. 12 Details of pressure contours near jet-air merge point at three flight Mach numbers. (Pressure contour interval is 2 kPa.)

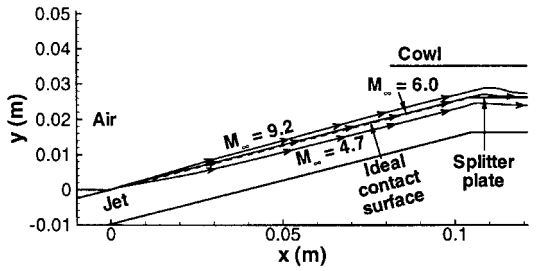

Fig. 13 Dividing streamlines at three flight Mach numbers showing displacement of contact surface for off-design conditions. (Ideal contact surface shown as – – –.)

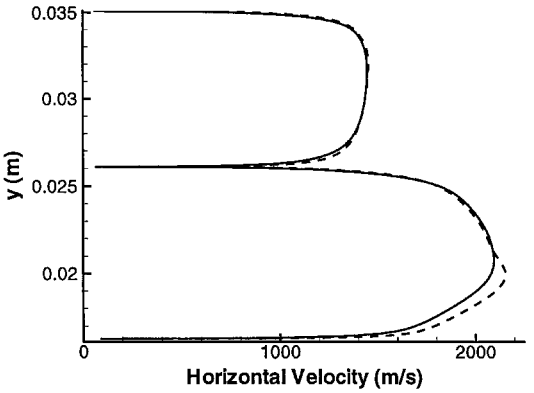

Fig. 14 Axial velocity profile comparison for baseline grid (——) and doubled grid (– – –) at an axial location 5 mm downstream of the leading edge of the splitter plate.

will match the angle of the airflow. This expansion reflects off the bottom wall and turns both flows parallel to the lower wall. Table 1 shows that the jet pressure was set higher than the air pressure behind the external shock so that pressures would be matched after the expansion waves.

Another effect of maintaining shock-on-lip is the displacement of the contact surface. This can most clearly be seen from streamline traces in the flowfields. The ideal contact surface would be a plane that extends from the merge point of the two streams downstream to the leading edge of the splitter plate. A streamline that began immediately below this surface would still be located immediately below the splitter plate downstream and similarly for one that began above the contact surface. Following a streamline that starts at the merge point, referred to here as a dividing streamline, will give a good indication of the actual location of the contact surface and the deviation from the ideal location.

At design conditions of a flight Mach number of 6, shown in Fig. 13, the dividing streamline indicates a contact surface that is coincident with the ideal. At a flight Mach number of 4.7, the dividing streamline is displaced downward soon after the merge point by the shock system that turns the jet flow. The flow returns to the initial direction parallel to the lower wall at the end of the jet shocks, but the displacement of the contact surface is maintained to the splitter plate. This displacement allows some of the air to spill below the splitter plate and represents a slight loss of compression and lost opportunity for heat addition. At a flight Mach number of 9.2, the dividing streamline is displaced upward soon after the merge point by the expansion fans that turn the jet flow. In this case some of the jet flow enters the isolator. This additional flow in the isolator has the beneficial effect of increasing the compression of the airstream that would somewhat counteract the effect of a nonoptimal splitter plate location. Free radicals in the jet, which may be present if the jet were produced by a combustion process, could help in initiating combustion in the combustor. The compression jet can also be used to inject some of the scramjet fuel in this way. For the conditions studied here the temperature along the contact surface is below the autoignition temperature; therefore, no reactions would occur. Significant changes in the flowfield would likely occur if reactions did take place in the shear layer. This issue would require further study. The displacement of the contact surface would need to be accounted for in a configuration with a moving splitter plate as just described.

Grid Resolution

To determine the adequacy of the grid spacing for the solutions just presented, a grid-doubling study was conducted. It was performed on the baseline case, which was for a flight Mach number of 6.0. The grid was doubled in both the axial and cross-stream directions, and Richardson's extrapolation was used to determine the maximum error. Profiles of axial velocity are shown in Fig. 14 for an axial location 5 mm downstream of the leading edge of the splitter plate (the location that exhibited the largest error). The largest error is approximately 3.4%, occurring in the compression jet about 3.5 mm above the lower wall. Throughout the majority of the flowfield, the error is less than 1%. Therefore, the grid spacing used in these cases is considered sufficiently small so that numerical resolution errors are not significant. This grid-doubling study was conducted using a nonadapted grid; however, for many of the cases the grid was adapted to cluster points near high gradients in pressure and velocity and increase the numerical accuracy.

Effect of Jet Parameters

The effect of the compression jet parameters on the inlet performance was also studied. In addition to the baseline jet Mach number of 2.0 and jet-to-air area ratio of 0.271, jet Mach numbers of 1.1 and 3.0 and a jet-to-air area ratio of 0.181 were investigated. The airflow was insensitive to these parameters, which is expected because the main effect of the jet is to provide a contact surface. Because the contact surface remains in the same location, the only change in the influence of the jet on the airstream is in the velocity ratio and convective Mach number between the streams, which influences the degree of mixing between the streams. For a freestream Mach number of 6 and jet Mach numbers or 1.1 and 3.0, the velocity ratios are 0.92 and 0.53, and convective Mach numbers are 0.075 and 0.99 respectively. Compared to a Mach 2 jet, more mixing occurs, and the shear layer is thicker for a Mach 3 jet because of the greater difference in velocity of the two streams, and less mixing occurs for the Mach 1.1 jet because the velocity ratio is close to one.

The changes in the jet parameters have two effects on the overall inlet characteristics. First, they change the mass-flow rate of stored propellants. Lower-Mach-number jets have a lower mass-flow rate for a given flow area. Decreasing the jet-flow area decreases the mass-flow rate of the jet. This is important for specific impulse calculations described next. Second, changing the jet-flow area changes the physical (jet-off) contraction ratio. As just stated, having a low physical contraction ratio can be advantageous, but this increases the mass-flow rate of the jet, which is detrimental to performance. These results indicate the jet-flow parameters could be modified to study their effects on overall performance without altering the inlet function. One such study is presented next.

Global Analysis of Potential Application

A global analysis was performed on the fluidic compression model. In this analysis the parameters of the compression jet are varied to estimate their effect on the inlet performance for fluidic compression. The analysis was done over a range of flight Mach numbers along the vehicle trajectory. A trajectory-dependent specific impulse based on a contraction ratio of 4 is used for the scramjet,[14] and the lower jet is assumed to be hydrogen gas at a stagnation temperature of 500 K or water vapor at a stagnation temperature of 3200 K, each with a specific impulse of 428 s. Using the mass-flow rates calculated for the compression jet and the inlet assuming full mass capture, the total specific impulse is calculated. This information is used to evaluate the effect of the jet Mach number, composition, and width on the total specific impulse at different flight Mach numbers. By assuming values of specific impulse for the airflow and the compression jet, the total specific impulse becomes an average of the two values, weighted by mass flow. Therefore, as the jet-flow rate approaches zero, the total specific impulse approaches the specific impulse of a scramjet with full mass capture.

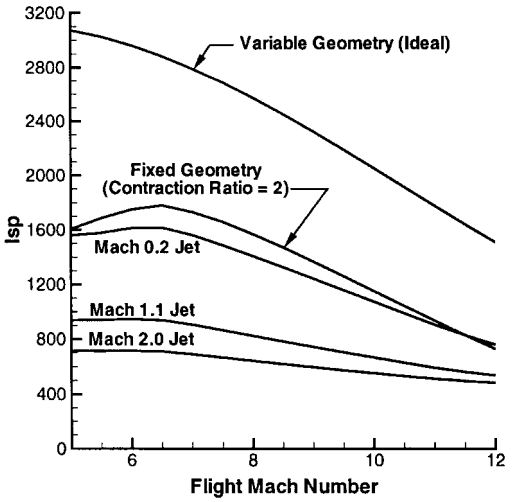

Fig. 15 Total specific impulse for fluidic compression inlet with jet-to-capture area ratio of 0.271 at several flight Mach numbers.

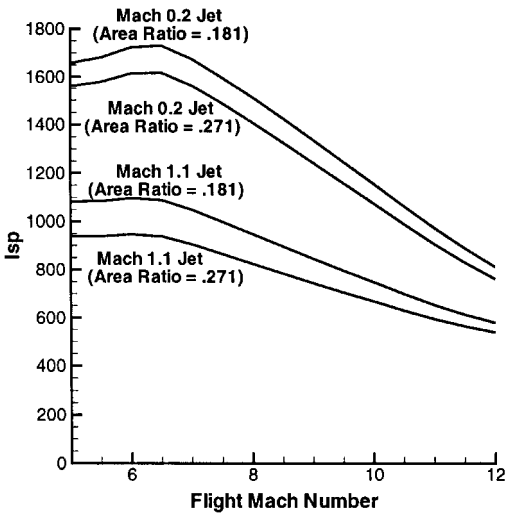

Fig. 16 Total specific impulse for fluidic compression inlet over range of flight Mach numbers at jet-to-capture area ratios of 0.181 and 0.271 at two jet Mach numbers.

Several important conclusions can be drawn from the global analysis. Figure 15 shows the effect of changing the jet Mach number on the specific impulse. The specific impulse for a variable geometry inlet[2] and a fixed geometry inlet with a contraction ratio of 2 is also shown.[14] The jet mass flow decreases with decreasing jet Mach number, with the highest specific impulse for the lowest-velocity compression jet. Because of the difference in temperature and specific heat between the hydrogen and water vapor jet, mass-flow rates and specific impulses are nearly identical. A preheated hydrogen compression jet would reduce the jet-mass-flow rate and increase specific impulse. However, if the hydrogen were to burn before reaching the splitter plate, as it would if it were above the autoignition temperature, the flowfield could change significantly, and the global analysis would not be applicable. No optimization has been performed on this inlet geometry; the performance would be significantly better if the fluidic compression inlet were designed for a much higher contraction ratio, such as 10. A subsonic jet was not studied numerically but was included here to assess the effect of a reduced mass-flow rate.

Figure 16 shows the total specific impulse for two different jet Mach numbers, each at two jet-flow areas. The jet mass flow decreases, and specific impulse increases with decreasing jet area. However, as the jet area decreases the engine flowpath is constricted, reducing low-Mach-number starting capability. If a low-blockage inlet is desired, this would not be the most advantageous way to reduce the jet-mass-flow rate. As the jet-flow area approaches zero, the inlet geometry approaches that of a higher-compression-ratio, fixed-geometry inlet.

These results indicate that minimizing the jet-mass-flow rate is critical for practical application of this concept. For the conditions specified, if the mass flow of the jet can be kept to less than 30% of the mass-flow rate of the fuel for the airstream, as in the Mach 0.2 case, then fluidic compression will be beneficial or neutral in specific impulse compared to a lower-compression conventional fixed geometry, but engine weight will be significantly less that of a variable-geometry inlet. One way the jet mass flow can be effectively reduced while maintaining an open engine flowpath is by reducing the jet Mach number. In addition, if some of the fuel for the scramjet can be introduced using the compression jet, the specific impulse penalty would be further reduced because that would reduce the amount of fuel injected downstream.

Conclusions

An inlet configuration, referred to as *fluidic compression*, which uses a fluid jet to compress the air has been analyzed using computational fluid dynamic models. In these models a jet of high-pressure gas injected at an angle to the main airflow is shown to compress supersonic air, with the contact surface between the air and the jet forming a virtual compression ramp.

By using fluidic compression, the minimum (jet-off) area of the flowpath is increased compared to a conventional fixed-geometry inlet. In the cases presented the capture stream tube is compressed with an area contraction ratio of 3.90, whereas the geometric contraction ratio is 1.87 for the current configuration. The flowpath could be opened further by altering the wall below the splitter plate, yielding an even lower geometric contraction ratio.

Shock-on-lip conditions can be maintained in a fixed-geometry configuration by adjusting the pressure of the compression jet; therefore, this is a highly controllable process. Another benefit of this inlet design is an elimination of the boundary-layer upstream of the isolator, which should reduce the risk of engine unstart. Disadvantages include the necessity of a splitter plate located in the high-speed flow and decreased overall specific impulse because of the mass flow used to supply the compression jet.

Using a jet to compress a supersonic airstream was demonstrated numerically. It results in a contact surface between the jet and the air and an external shock that compresses the air. Some mixing occurs between these two streams, which eliminates the boundary layer in the air before the isolator. At off-design flight Mach numbers changing the jet pressure was demonstrated to successfully maintain shock-on-lip conditions, resulting in full air mass capture and preventing overspeeding. The contact surface shifts position at different flight Mach numbers. Sufficient numerical resolution was demonstrated by the solution on a doubled grid.

Although the thickness and speed of the compression jet had little effect on the airstream, the results of a global analysis suggest that the jet flow should be minimized in order to minimize the additional propellant needed and improve specific impulse. Reducing the jet flow can be accomplished most effectively by reducing the Mach number or density of the compression jet.

Acknowledgments

This work was supported by the NASA John H. Glenn Research Center at Lewis Field, Contract NAS3-97020, through a subcontract from TEKNOS. The authors would like to especially thank Richard Foster of TEKNOS, Fred Billig of Pyrodyne, and Mel Bulman of Aerojet for discussions and input on this work.

References

[1]Ferri, A., "Mixing-Controlled Supersonic Combustion," *Annual Review of Fluid Mechanics*, Vol. 5, 1973, pp. 310–308.

[2]Foster, R., Escher, W., and Robinson, J., "Studies of an Extensively Axisymmetric Rocket Based Combined Cycle (RBCC) Engine Powered SSTO Vehicle," AIAA Paper 89-2294, July 1989.

[3]Curran, E., Heiser, W., and Pratt, D., "Fluid Phenomena in Scramjet Combustion Systems," *Annual Review of Fluid Mechanics*, Vol. 28, 1996, pp. 323–360.

[4]Pulliam, T., and Chaussee, D., "A Diagonal Form of an Implicit Approximate-Factorization Algorithm," *Journal of Computational Physics*, Vol. 39, No. 2, 1981, pp. 347–363.

[5]Pulliam, T. H., "Efficient Solution Methods for the Navier–Stokes Equations," Numerical Techniques for Viscous Flow Computation in Turbomachinery Bladings, Lecture Notes, von Kármán Inst., Rhode-St-Genese, Belgium, 1985.

[6]Towne, C., and Jones, R., "Results and Current Status of the NPARC Alliance Validation Effort," AIAA Paper 96-0387, Jan. 1996.

[7]Bush, R., Power, G., and Towne, C., "WIND: The Production Flow Solver of the NPARC Alliance," AIAA Paper 96-0935, Jan. 1996.

[8]Choi, D., and Barber, T., "Large Eddy Simulations of High-Reynolds Number Jet Flows," AIAA Paper 99-0230, Jan. 1999.

[9]Buelow, P. E., Schwer, D. A., Feng, J., Merkle, C. L., and Choi, D., "A Preconditioned Dual-Time, Diagonalized ADI Scheme for Unsteady Computations," AIAA Paper 97-2101, June 1997.

[10]Coakley, T., and Huang, P., "Turbulence Modeling for High Speed Flows," AIAA Paper 92-0436, Jan. 1992.

[11]Dutton, J., "Compressible Turbulent Free Shear Layers," Rept. 819, AGARD, June 1997.

[12]Wilcox, D., *Turbulence Modeling for CFD,* DCW Industries, Inc., La Cañada, CA, 1994, pp. 183–189.

[13]Russell, R., Brocco, D., and Daines, R., "Modeling and Validation of an Ejector Primary Rocket for Shielded Afterburning Fuel Injection," AIAA Paper 99-2241, June 1999.

[14]Billig, F., Orth, R., and Lasky, M., "Effects of Thermal Compression on the Performance Estimates of Hypersonic Ramjets," *Journal of Spacecraft and Rockets*, Vol. 5, No. 4, 1968, pp. 1076–1081.

M. Torres
Associate Editor